Lewis 830-H-15
NASA 1.60:1620
NASA 160
JUN 12 1980
COMPLETED
ORIGINAL

NASA Technical Paper 1620

Flutter Analysis of an Airplane With Multiple Structural Nonlinearities in the Control System

Elmar J. Breitbach

MARCH 1980

NASA

39

NASA Technical Paper 1620

Flutter Analysis of an Airplane With Multiple Structural Nonlinearities in the Control System

Elmar J. Breitbach
Langley Research Center
Hampton, Virginia

National Aeronautics
and Space Administration

**Scientific and Technical
Information Office**

1980

SUMMARY

Experience has shown that the flutter prediction process for airplanes can be greatly affected by strong concentrated nonlinearities which may be localized in the linking elements of the control mechanism, in the pivot joints of variable-sweep-wing systems, and in the connecting points between wing- and pylon-mounted external stores. The principle of equivalent linearization offers an efficient possibility for solving the related nonlinear flutter equations in the frequency domain as a complement to the well-known time domain procedures. Taking as an example an airplane with nonlinear control characteristics, it is demonstrated how the equivalent linearization approach can be extended to rather complicated systems with multiple sets of strongly interacting, concentrated nonlinearities.

INTRODUCTION

Routine flutter analyses generally imply linearized representation of both the structural and the aerodynamic properties. This approximation has proved to be a useful basis for the flutter clearance of a large number of aircraft prototypes. There remains, nevertheless, a significant number of flutter cases suffering from rather poor agreement between analysis and test results. Many of these disagreements can be traced to structural nonlinearities. A survey of the various types of structural nonlinearities, their physical sources, and their effects on aircraft vibration and flutter is given in reference 1, which indicates that strong concentrated nonlinearities are a common feature of the control systems of mechanically controlled airplanes. From reference 2, which presents a new experimental-numerical approach to determining the dynamic characteristics of hydraulic aircraft control actuators, it becomes obvious that flutter of aircraft with hydraulic controls may also be greatly affected by strong concentrated nonlinearities. References 3 and 4 focus on the special case of a modern variable-sweep-wing fighter airplane with concentrated nonlinearities in the wing pivot mechanism and in the corresponding single-point external store suspension system. Reference 5 and, in particular, reference 6 describe several concepts of how the governing equations of airplanes with control system nonlinearities can conveniently be formulated in terms of consistent sets of both measured modal data and nonlinear force-deflection diagrams. The nonlinear flutter equations can be solved in the time domain by using analog computer techniques (see refs. 5 and 7) or by numerical integration. In addition to this time domain approach, promising attempts have been made to solve nonlinear flutter problems in the frequency domain by employing the principle of equivalent linearization (see ref. 8). The effectiveness and accuracy of this equivalent linearization approach were impressively demonstrated for a semispan wing-aileron model with a single nonlinearity in the aileron hinge; the calculated and the wind-tunnel test results agreed very well (see ref. 1).

Application of the equivalent linearization approach to systems with more than one nonlinearity creates some additional, though still solvable, difficul-

ties. These difficulties are associated with an incompatibility between the input data representing the equivalent stiffness and damping properties of the nonlinearities involved and the corresponding output deflections. In coping with this problem, a recent investigation (ref. 9) describes the application of a method called the describing function method[1] (ref. 10) to the special case of a flexible missile control surface with simple undamped free-play nonlinearities in both the roll and pitch degree of freedom of the root support stiffness.

The particular concern of the present study is the extension of the equivalent linearization concept to the flutter analysis of complete airplanes with strong hysteresis-type nonlinearities in the control system. Antisymmetrical flutter of a sailplane involving strongly interacting rudder and aileron nonlinearities is used as a realistic example to demonstrate the applicability of the method proposed.

SYMBOLS

A,B,C	mass, damping, and stiffness matrices, respectively, defined in terms of physical deflections
$\Delta A,\Delta B,\Delta C$	matrices of mass, damping, and stiffness changes, respectively, defined in terms of physical deflections
b	viscous damping coefficient of control surface hinge
c	stiffness coefficient of control surface hinge
f	frequency, $\omega/2\pi$
F	force or moment acting on control surface
g	absolute amplitude value, see equation (31)
h	bending deflection of quarter-chord line of lifting surface
j	imaginary unit, $\sqrt{-1}$
ℓ	half-chord length
M_f	flight Mach number
M,D,K	generalized mass, damping, and stiffness matrices, respectively
$\Delta M,\Delta D,\Delta K$	generalized matrices of mass, damping, and stiffness changes, respectively

[1] A slightly modified form of the equivalent linearization approach.

N	number of controls involved in flutter case
P	column matrix of external forces
q	column matrix of generalized coordinates
Q	column matrix of generalized forces
R	matrix of unsteady aerodynamic forces R_r related to normal modes Φ_r
t	time
u	column matrix of physical deflections
V	flight speed
α	rotation about quarter-chord line of lifting surface
β	control surface rotation about hinge line
γ	damping loss angle, 2ζ
Γ	diagonal matrix of damping loss angles
ϵ	matching function, see equation (30)
ζ	damping expressed as ratio to critical damping
η	absolute amplitude value, see equation (29)
Λ	diagonal matrix of square values of circular normal frequencies $\omega_r = 2\pi f_r$
ρ	air density
τ	control surface chord length ratio (see fig. 11)
ϕ	integration variable, ωt
Φ	modal matrix of normal modes Φ_r
ω	circular frequency

Subscripts:

A	aileron properties
L	linear properties
NL	nonlinear properties

r normal mode index, $r = 1, 2, \ldots, n$

R rudder properties

ν,μ,σ indices of concentrated nonlinearities involved

Superscripts:

F flutter speed

T transposed matrix

0 starting values

NONLINEAR EQUATIONS OF MOTION

Reference 6 offers a choice of several modal synthesis concepts which can conveniently be used to establish the aeroelastic equations of motion for the flutter analysis of airplanes with strong concentrated control system nonlinearities. In accordance with one of these concepts (concept II of ref. 6), the originally nonlinear airplane structure is physically converted to an artificially linearized test configuration by replacing the nonlinear elements by linear stiffnesses with low damping. The normal mode characteristics of the linearized test configuration serve as a consistent basis for the calculation of both the unsteady aerodynamic reactions and a set of nonlinear coupling terms retransforming the test configuration to the actual system. The nonlinearities can be determined statically in the form of force-deflection diagrams or dynamically by direct measurement of equivalent stiffness and damping values versus vibration amplitude. The equations of motion of the modified linearized test configuration, formulated in terms of physical deflections, can be written in matrix notation as follows:

$$A\ddot{u} + B_L\dot{u} + C_L u = P \tag{1}$$

where

A mass matrix

B_L viscous damping matrix

C_L stiffness matrix

P column matrix of external forces, for instance, unsteady aerodynamic forces

u column matrix of physical deflections; $\dot{u}$ and $\ddot{u}$ are first- and second-order differentials with respect to time t

The dynamic behavior of the unchanged nonlinear system may be described by

$$A\ddot{u} + B\dot{u} + Cu = P \tag{2}$$

where

$$\left.\begin{aligned} B &= B_L - \Delta B_L + \Delta B_{NL} \\ C &= C_L - \Delta C_L + \Delta C_{NL} \end{aligned}\right\} \tag{3}$$

and where ΔC_L and ΔB_L denote the stiffness and damping properties of the artificial linear elements and ΔC_{NL} and ΔB_{NL} denote the amplitude-dependent stiffness and damping of the replaced nonlinearities.

Development of the arbitrary deflection vector u in a series expansion of the normal modes Φ_r of the linearized test configuration yields

$$u = \Phi q \tag{4}$$

where

Φ modal matrix containing normal modes Φ_r as columns

q column vector of generalized coordinates

Substituting the modal transformation (eq. (4)) into equation (2), premultiplying by Φ^T, and taking into account equation (3) lead to the generalized equations of motion of the unmodified nonlinear system

$$M\ddot{q} + (D_L - \Delta D_L + \Delta D_{NL})\dot{q} + (K_L - \Delta K_L + \Delta K_{NL})q = Q \tag{5}$$

where

$$\left.\begin{aligned} M &= \Phi^T A \Phi \\ D_L &= \Phi^T B_L \Phi \\ \Delta D_{NL} - \Delta D_L &= \Phi^T (\Delta B_{NL} - \Delta B_L) \Phi \\ K_L &= \Phi^T C_L \Phi \\ \Delta K_{NL} - \Delta K_L &= \Phi^T (\Delta C_{NL} - \Delta C_L) \Phi \\ Q &= \Phi^T P \end{aligned}\right\} \tag{6}$$

Consider the νth of N controls involved in a flutter case; the corresponding part of the modal matrix Φ degenerates to the row matrix

$$\Phi_\nu = [\beta_{\nu 1}, \beta_{\nu 2}, \ldots, \beta_{\nu r}, \ldots, \beta_{\nu n}] \tag{7}$$

with $\beta_{\nu r}$ denoting the control rotation in the section where the control force is applied. Accordingly, the matrices $\Delta B_{NL} - \Delta B_L$ and $\Delta C_{NL} - \Delta C_L$ degenerate to the 1×1 matrices

$$\left.\begin{aligned} \Delta B_{NL,\nu} - \Delta B_{L,\nu} &= b_{NL,\nu}(\beta_\nu) - b_{L,\nu} \\ \Delta C_{NL,\nu} - \Delta C_{L,\nu} &= c_{NL,\nu}(\beta_\nu) - c_{L,\nu} \end{aligned}\right\} \tag{8}$$

where $c_{L,\nu}$ and $b_{L,\nu}$ define the artificial hinge stiffness and damping of the νth control surface and $c_{NL,\nu}(\beta_\nu)$ and $b_{NL,\nu}(\beta_\nu)$ define the amplitude-dependent stiffness and damping of the replaced nonlinearity of the νth control surface. Hence,

$$\left.\begin{aligned} \Delta D_{NL} - \Delta D_L &= \sum_{\nu=1}^{N} (\Delta D_{NL,\nu} - \Delta D_{L,\nu}) = \sum_{\nu=1}^{N} \Phi_\nu{}^T [b_{NL,\nu}(\beta_\nu) - b_{L,\nu}]\Phi_\nu \\ \Delta K_{NL} - \Delta K_L &= \sum_{\nu=1}^{N} (\Delta K_{NL,\nu} - \Delta K_{L,\nu}) = \sum_{\nu=1}^{N} \Phi_\nu{}^T [c_{NL,\nu}(\beta_\nu) - c_{L,\nu}]\Phi_\nu \end{aligned}\right\} \tag{9}$$

The normal modes Φ_r of the linearized test configuration satisfy the orthogonality condition,

$$\begin{aligned} \Phi^T A \Phi &= M \\ \Phi^T C_L \Phi &= \Lambda_L M = K_L \end{aligned} \tag{10}$$

where

M diagonal matrix of generalized masses M_r

K_L diagonal matrix of generalized stiffnesses $K_{L,r} = \omega_{L,r}^2 M_r$

Λ_L diagonal matrix of square values of circular normal frequencies $\omega_{L,r}$

The generalized damping matrix D_L, which is not necessarily diagonal, was defined in equation (6). Without damping coupling, matrix D_L also becomes diagonal with the generalized damping elements $D_{L,r}$.

The unsteady aerodynamic forces P generally depend on time t, flight Mach number M_f, flight speed V, and air density ρ. Developing P in a series expansion of unsteady aerodynamic forces R_r related to the normal modes Φ_r leads to

$$Q = \Phi^T R(M_f, V, \rho, t)\, q \tag{11}$$

where

$$R(M_f, V, \rho, t) = [R_1, R_2, \ldots, R_r, \ldots, R_n] \tag{12}$$

As mentioned previously, application of the equivalent linearization approach to nonlinear flutter problems requires a transformation of the differential equation (5) into the frequency domain. Accordingly, by assuming simple harmonic motions,

$$q(t) = qe^{j\omega t} \qquad (j = \sqrt{-1}) \qquad (13)$$

where ω is the circular frequency, equation (5) reduces to

$$[-\omega^2 M + j\omega(D_L - \Delta D_L + \Delta D_{NL}) + K_L - \Delta K_L + \Delta K_{NL} - \Phi^T R(M_f, V, \rho, \omega)]q = 0 \qquad (14)$$

Solutions of this equation can be obtained much more easily by expressing the viscous damping forces in terms of complex stiffnesses or damping loss angles. By so doing, equation (14) becomes

$$\left\{-\omega^2 M + j\left[\Gamma K_L - \sum_{\nu=1}^{N} \gamma_{L,\nu}\, \Delta K_{L,\nu} + \sum_{\nu=1}^{N} \gamma_{NL,\nu}(\beta_\nu)\, \Delta K_{NL,\nu}\right]\right.$$

$$\left. + K_L - \Delta K_L + \Delta K_{NL} - \Phi^T R(M_f, V, \rho, \omega)\right\}q = 0 \qquad (15)$$

Damping can also be expressed by ζ as a ratio to the critical damping. The relation between ζ and γ is $\zeta = \gamma/2$. In equation (15), Γ denotes the diagonal matrix of the damping loss angles γ_r associated with the generalized stiffnesses K_r. The matrices $\Delta K_{L,\nu}$ and $\Delta K_{NL,\nu}$ are defined in equation (9). The damping loss angles $\gamma_{L,\nu}$ and $\gamma_{NL,\nu}(\beta_\nu)$ represent the structural damping coefficients associated with the hinge stiffnesses $c_{L,\nu}$ and $c_{NL,\nu}(\beta_\nu)$, respectively, which are defined in equation (8). The matrices M, Γ, Λ_L, and Φ, which describe the dynamic behavior of the modified linearized system, can be measured in a fairly simple ground vibration test (GVT). These modal data and some related geometrical data are given in detail in appendix A for the sailplane taken as an example of a nonlinear system. Because of the high aspect ratio and the comparatively low maximum speed of this sailplane, incompressible strip theory is used to calculate the unsteady aerodynamic forces based on the measured mode shapes Φ_r. The method of determining the nonlinear terms $\gamma_{NL,\nu}(\beta_\nu)$ and $\Delta K_{NL,\nu}$ is described in the following section.

EQUIVALENT LINEARIZATION APPROACH

As is known from reference 8, an elastodynamic system with nonlinear stiffness and damping elements can be approximately described as a linear system for constant-amplitude vibrations at any arbitrary amplitude level. The fundamental idea of this equivalent linearization approach is based on the assumption that a nonlinear elastomechanical element can be approximately replaced by a linear substitute element with equivalent stiffness and damping energies when activated at equivalent amplitude levels. The accuracy of the approach, depending on the special problem to be investigated, can be assessed by procedures described, for instance, in references 11 and 12 for application to systems subjected to simple harmonic excitation. In addition, reference 12 shows a simple way to solve problems with preloaded nonsymmetric nonlinearities, such as those arising in systems subjected to maneuver loads.

In accordance with reference 8 the equivalent linear coefficients of a nonlinear force-deflection diagram can be calculated from

$$\left.\begin{aligned} c_{NL}(\beta) &= \frac{1}{\pi\beta}\int_{\phi=0}^{2\pi} F(\beta\cos\phi, -\beta\omega\sin\phi)\cos\phi\,d\phi \\ \gamma_{NL}(\beta) &= -\frac{1}{c_{NL}(\beta)\,\pi\beta}\int_{\phi=0}^{2\pi} F(\beta\cos\phi, -\beta\omega\sin\phi)\sin\phi\,d\phi \end{aligned}\right\} \tag{16}$$

where $c_{NL}(\beta)$ and $\gamma_{NL}(\beta)$ define the complex stiffness,

$$c^{*}_{NL}(\beta) = c_{NL}(\beta)[1 + j\,\gamma_{NL}(\beta)] \tag{17}$$

and where the force F is a nonlinear function of the deflection β. Integration is carried out over a full period of oscillation using $\phi = \omega t$ as integration variable.

In view of the particular flutter case to be dealt with subsequently, two special types of bilinear force-deflection diagrams, sketched in figures 1 and 2, are evaluated by means of equation (16). The diagram in figure 1 is characterized by a low stiffness c_1 for

$$-\beta_1 \leq \beta \leq \beta_1 \tag{18}$$

where β_1 denotes the amplitude corresponding to the maximum stroke of the control surface. For

$$-\beta_1 > \beta > \beta_1 \tag{19}$$

the stiffness assumes the much higher value c_2 because of kinematic limitation beyond the blocking point (see figs. 1 and 2). Hence it follows that

$$\left.\begin{aligned} c_{NL}(\beta) &= c_2\left[1 - \frac{1}{\pi}\left(1 - \frac{c_1}{c_2}\right)(\sin 2\phi_1 + 2\phi_1)\right] \\ \gamma_{NL}(\beta) &= 0 \end{aligned}\right\} \tag{20}$$

where

$$\phi_1 = \arcsin\frac{\beta_1}{\beta} \tag{21}$$

Figure 2 illustrates a bilinear hysteresis-type force-deflection diagram. For amplitudes below the blocking point according to equation (18), the equivalent stiffness and damping values are

$$\left.\begin{aligned} c_{NL}(\beta) &= \frac{c_2}{2\pi}(2\phi_1 - \sin 2\phi_1) \\ \gamma_{NL}(\beta) &= \frac{2 \sin^2 \phi_1}{2\phi_1 - \sin 2\phi_1} \end{aligned}\right\} \tag{22}$$

where

$$\phi_1 = \arccos\left(1 - \frac{2F_0}{c_2\beta}\right) \tag{23}$$

where F_0 is defined in figure 2. For amplitudes beyond the blocking point according to equation (19), the equivalent stiffness and damping values are

$$\left.\begin{aligned} c_{NL}(\beta) &= \frac{c_2}{2\pi}(2\phi_1 - 2\phi_2 + \pi - \sin 2\phi_1 - \sin 2\phi_2) \\ \gamma_{NL}(\beta) &= \frac{\cos 2\phi_1 + \cos 2\phi_2}{2\phi_1 - 2\phi_2 + \pi - \sin 2\phi_1 - \sin 2\phi_2} \end{aligned}\right\} \tag{24}$$

where

$$\left.\begin{aligned} \phi_1 &= \arccos \frac{2\beta_0 - \beta_1}{\beta} \\ \phi_2 &= \arcsin \frac{\beta_1}{\beta} \end{aligned}\right\} \tag{25}$$

where β_0 is defined in figure 2.

SOLUTION OF THE NONLINEAR FLUTTER EQUATIONS

Equation (15), which is usually written in the form of a complex eigenvalue problem, can be solved for an arbitrary set of N equivalent stiffness and damping values $c^0_{NL,\nu}(\beta_\nu)$ and $\gamma^0_{NL,\nu}(\beta_\nu)$ which, because of their amplitude dependency, correspond to a definite set of deflections $\beta_\nu{}^0$. Standard flutter calculation techniques can be applied to determine the flutter boundary which is generally characterized by an undamped harmonic oscillation of one of the generalized degrees of freedom. The corresponding generalized eigenvector $q_r{}^F$ can be transformed into the physical deflections:

$$u^F = \Phi q_r{}^F \tag{26}$$

The deflections $\beta_\nu{}^F$ of the different control surfaces with nonlinear elements which are part of the flutter mode shape u^F can be determined by

$$\beta_\nu{}^F = \Phi_\nu q_r{}^F \qquad (\nu = 1, 2, \ldots, N) \qquad (27)$$

The deflections $\beta_\nu{}^F$ represent a consistent set of solutions if and only if the following condition is satisfied:

$$\eta_\nu{}^F - \eta_\nu{}^0 = 0 \qquad (\nu = 1, 2, \ldots, N) \qquad (28)$$

where

$$\eta_\nu{}^0 = |\beta_\nu{}^0| \qquad \eta_\nu{}^F = |\beta_\nu{}^F| \qquad (29)$$

In fulfilling condition (28), the following iterative procedure may be employed. In a first step a set of amplitudes $\eta_\nu{}^0$ corresponding to a set of equivalent stiffness and damping values $c^0_{NL,\nu}$ and $\gamma^0_{NL,\nu}$, respectively, is selected as input data for an initial flutter calculation. At the flutter speed resulting from this calculation, the related flutter mode deflections $\beta_\nu{}^F$ can be calculated by means of equation (27). The difference between the initial amplitudes $\eta_\nu{}^0$ and the flutter mode amplitudes $\eta_\nu{}^F$, both of which are defined by equation (29), can be set into the more extended form

$$\varepsilon = \sum_{\nu=1}^{N} (g_\nu{}^F - \eta_\nu{}^0)^2 \equiv 0 \qquad (30)$$

where

$$g_\nu{}^F = \frac{\eta_\nu{}^F \eta_\mu{}^0}{\eta_\mu{}^F} \qquad (\nu = 1, 2, \ldots, N) \qquad (31)$$

which means that the amplitude of the μth nonlinear element is kept constant for all further calculations; that is,

$$g_\mu{}^F = \eta_\mu{}^0 \qquad (32)$$

To determine an optimal change $\Delta\eta_\nu$ of the starting values $\eta_\nu{}^0$ for the next iteration step, ε is successively differentiated with respect to the amplitudes $\eta_\nu{}^0$:

$$\frac{\partial \varepsilon}{\partial \eta_\nu{}^0} = -2(g_\nu{}^F - \eta_\nu{}^0) + 2 \sum_\sigma (g_\sigma{}^F - \eta_\sigma{}^0) \frac{\partial g_\sigma{}^F}{\partial \eta_\nu{}^0}$$

$$(\sigma = 1, 2, \ldots, \mu-1, \mu+1, \ldots, N; \quad \nu = 1, 2, \ldots, \mu-1, \mu+1, \ldots, N) \qquad (33)$$

The gradients $\partial\varepsilon/\partial\eta_\nu{}^0$ can be approximately determined by successive small changes of the values $\eta_\nu{}^0$ resulting in N - 1 flutter calculations. To insure that each succeeding iteration step is going in an optimal direction, signs of the changes $\Delta\eta_\nu$ have to be chosen as follows:

$$\text{sign } (\Delta\eta_\nu) = -\text{sign}\left(\frac{\partial\varepsilon}{\partial\eta_\nu{}^0}\right) \tag{34}$$

where the finite differences $\Delta\eta_\nu$ are much larg than those used for the determination of the gradient $\partial\varepsilon/\partial\eta_\nu{}^0$. In app ching condition (30), it may be found that the difference $\eta_\nu{}^F - \eta_\nu{}^0$ chan sign. In this case, the next change $\Delta\eta_\nu$ can be determined by interpolati between the two successive values of $\eta_\nu{}^F - \eta_\nu{}^0$. Consequently, the changes $\Delta\eta_\nu$ for the next iterations have to be reduced to fractions of the last value of $\Delta\eta_\nu$ found by interpolation. The procedure as described above can be iteratively repeated until equation (28) is fulfilled (i.e., a matching point is obtained). Figures 3 and 4 give two examples of the functions $\eta_\nu{}^F - \eta_\nu{}^0$ and ε.

Despite the comparatively large number of flutter calculations during the iteration process, the numerical effort in terms of computer time remains low because only one set of normal modes is required. Consequently, only one corresponding set of unsteady aerodynamic forces is necessary. The applicability of the proposed approach is demonstrated in the following section for the example of a sailplane system with two complicated nonlinearities.

APPLICATION TO CONTROL SYSTEM NONLINEARITIES OF A SAILPLANE

Description of Cases Studied

To obtain a better insight into the mechanism of nonlinear flutter, three different configurations distinguished by different kinds of nonlinearities in the rudder and aileron control system of a sailplane are investigated. As a basis for selecting these configurations, some nonlinear data measured on the sailplane in dynamic and static tests are available. Thus, the nonlinear characteristics of the aileron system can be derived from a statically measured force-deflection diagram (fig. 5) and from the dynamically measured aileron resonance frequency as a function of the amplitude β_A (fig. 6). The nonlinear properties of the rudder system are available in the form of the statically measured force-deflection diagram in figure 7 with the standard trim stiffness removed. The special features of the three configurations can be described as follows:

Configuration I.- To assess the importance of strong hysteretic damping on flutter behavior, damping is eliminated in this configuration.

Configuration II.- In this configuration the actual nonlinearities with measured hysteretic damping are taken into account, but the standard trim stiffness of the rudder system is eliminated.

Configuration III.- The rudder and aileron system nonlinearities of this configuration are equivalent to those of the functionally complete sailplane including the rudder trim stiffness.

The numerical values quantitatively describing the three configurations are detailed in appendix B.

Results

The nonlinear flutter boundaries of configurations I, II, and III are depicted in figures 8, 9, and 10 in the form of the amplitude ratios $\eta_A^F/\beta_{1,A}$ and $\eta_R^F/\beta_{1,R}$ as functions of the flight speed. Figure 8 shows that the artificial configuration without damping results in a linear flutter behavior with a flutter speed independent of amplitude up to the blocking point at the kinematic limit ($\eta_R^F/\beta_{1,R} = 1$). Above that amplitude, the flutter speed drops sharply as the amplitude further increases. This configuration has been investigated to form a basis for demonstrating the effects of nonlinear hysteretic damping such as that inherent in the more realistic configurations II and III to be discussed next.

As shown in figure 9, the influence of hysteretic damping results in a considerable stabilizing effect compared with configuration I. This means that between 195 and 235 km/hr, the nonlinear flutter boundary is characterized by increasing flutter speed as the amplitude ratios $\eta_R^F/\beta_{1,R}$ and $\eta_A^F/\beta_{1,A}$ decrease. However, the system at speeds within the above given range is stable only below a certain amplitude level, which can easily be exceeded by external excitation due to gust or maneuver loads resulting in violent divergent flutter. This special type of nonlinear flutter is contradictory to the wide-spread opinion that the effect of structural nonlinearities on flutter results always in limit cycle flutter vibrations.

The functionally complete sailplane with a trim stiffness in the rudder control system is investigated in configuration III. As shown in figure 10, the additional spring stiffness results in considerable destabilization compared with configurations I and II. In a comparatively large speed range between 180 and 225 km/hr, external perturbations of not more than about 50 percent of the blocking amplitudes of both the aileron and the rudder are sufficient to induce violent flutter.

As for experimental verification of this flutter behavior, it is worth mentioning that some time before the first routine flutter clearance on the basis of GVT and flutter calculations, a number of flight flutter tests were accomplished. The most remarkable result of these tests was found at about 180 km/hr. According to test pilot reports and observations from the ground, extremely lowly damped free vibrations with large amplitudes could be excited by pilot-induced rudder oscillations at an estimated frequency of between 3 and 5 Hz, which forced the rudder to amplitudes near the blocking amplitude. On

the basis of figure 10, a small increment in speed would have resulted in violent flutter. It should be mentioned that the flutterlike vibrations were eliminated by mass-balancing the rudder.

CONCLUDING REMARKS

Based on standard flutter calculation techniques in the frequency domain and on the equivalent linearization approach, a method has been developed to predict the flutter behavior of complete airplanes with multiple sets of concentrated nonlinearities. The applicability of the method has been demonstrated for the example of antisymmetrical flutter of a sailplane with nonlinearities in its control systems. The results are in good agreement with observations during actual flight tests of the sailplane.

In future investigations, emphasis should be placed on the following problems:

1. Investigation of service-life-dependent alterations of concentrated structural nonlinearities

2. Investigation of mass, damping, and stiffness alterations due to pilot feedback

3. Amendment of ground vibration test methods and flight and wind-tunnel flutter test techniques by paying more attention to nonlinear effects

4. Development of suitable methods for the calculation of unsteady aerodynamic forces in the time domain for all flight speed ranges

5. Application of digital and analog time domain techniques to solve transient problems such as those due to gust loads, maneuver loads, and sudden failure of control system devices

6. Investigation of the frequency-dependent dynamic properties of nonlinear elements

7. Investigation of nonlinear effects on design, test, and operation of flutter suppression and vibration reduction systems

Langley Research Center
National Aeronautics and Space Administration
Hampton, VA 23665
February 8, 1980

APPENDIX A

MODAL DATA OF A SAILPLANE IN A MODIFIED LINEARIZED TEST CONFIGURATION

To obtain a largely linear test configuration, the nonlinear elements in the aileron, rudder, and elevator control mechanisms of a sailplane were replaced by linear lowly damped spring elements. A sketch of the sailplane investigated and the strip arrangement used to calculate the unsteady aerodynamic forces is shown in figure 11. Tables I, II, and III list the five lowest antisymmetrical normal modes and the geometrical data of the strip scheme. As shown in figure 11, the normal mode displacements referring to the midstrip sections are split up into the quarter-chord point bending deflection h, torsion α, and control surface rotation β. The generalized masses M_r, the normal frequencies $f_r = \omega_r/2\pi$, and the damping loss angles γ_r are listed in table IV.

Since this investigation is of an antisymmetrical flutter case, only the rudder control system and the aileron control system must be taken into account. Correspondingly, in accordance with equation (7), only the row matrices Φ_R and Φ_A describing the antisymmetrical hinge rotation angles $\beta_{R,r}$ and $\beta_{A,r}$ of the rudder and the aileron (ν = R,A) are given in table V.

APPENDIX B

QUANTITATIVE DETERMINATION OF NONLINEAR CHARACTERISTICS OF CONFIGURATIONS I, II, AND III

Configuration I

The following values are chosen for describing the nonlinearities of both the rudder and the aileron system by bilinear zero damping force-deflection diagrams such as those shown in figure 1:

$c_{1,A} = 10$ N-m/rad $\qquad c_{1,R} = 0$

$c_{2,A} = 500$ N-m/rad $\qquad c_{2,R} = 500$ N-m/rad

$\beta_{1,A} = 20^{\circ} \qquad \beta_{1,R} = 30^{\circ}$

The stiffnesses $c_{2,A}$, $c_{1,R}$, and $c_{2,R}$ are estimated from figures 5 and 7, respectively. Stiffness $c_{1,A}$ can be approximately calculated from

$$c_{1,A} = \frac{M_2}{2}(2\bar{\tau}_A\bar{\ell})^2(2\pi f_{A,min})^2 \tag{B1}$$

where

M_2 generalized mass of normal mode $r = 2$ (see table IV)

$\bar{\tau}_A$ ratio of aileron chord length to wing chord length at inboard edge of aileron

$\bar{\ell}$ half-chord length of the wing at inboard edge of aileron

$f_{A,min}$ minimum resonance frequency of aileron system (see fig. 6)

Application of equation (B1) implies that the normal mode $r = 2$ fundamentally consists of motion of the aileron system (see tables I, II, and III). The equivalent stiffnesses $c_{NL,A}(\beta)$ and $c_{NL,R}(\beta)$ of the aileron and the rudder system calculated by means of equation (20) are shown in figure 12.

Configuration II

This configuration is characterized by hysteresis-type force-deflection diagrams in both the aileron and the rudder system. The force-deflection diagram of the rudder system shown in figure 7 can be approximated by a bilinear diagram of the kind sketched in figure 2. Because the trim stiffness is eliminated in this configuration, the following quantitative data can be selected:

APPENDIX B

$c_{1,R} = 0$ $\beta_{1,R} = 30^{o}$

$c_{2,R} = 500$ N-m/rad $F_{0,R} = 7$ N-m

The corresponding equivalent stiffness and damping functions $c_{NL,R}(\beta)$ and $\gamma_{NL,R}(\beta)$ are plotted in figure 13. The equivalent aileron stiffness $c_{NL,A}(\beta)$ can be calculated from

$$c_{NL,A}(\beta) = \frac{M_2}{2}(2\bar{\tau}_A\bar{\ell})^2[2\pi\ f_A(\beta)]^2 \qquad \text{(B2)}$$

The terms M_2, $\bar{\tau}_A$, and $\bar{\ell}$ are already defined with equation (B1). Figure 6 shows the resonance frequency $f_A(\beta)$ of the aileron system measured as a function of β. The equivalent aileron damping loss angle can be calculated approximately from

$$\gamma_{NL,A}(\beta) = \frac{4F_{0,A}}{\pi\ c_{NL,A}(\beta)\beta} \qquad (\beta \leq \beta_{1,A}) \qquad \text{(B3)}$$

and

$$\gamma_{NL,A}(\beta) = \frac{4F_{0,A}\beta_{1,A}}{c_{NL,A}(\beta)\beta^2} \qquad (\beta < \beta_{1,A}) \qquad \text{(B4)}$$

where

$F_{0,A} = 0.283$ N-m

The terms $c_{NL,A}(\beta)$ and $\gamma_{NL,A}(\beta)$ are plotted in figure 14.

Configuration III

The aileron characteristics of this configuration are equivalent to those of configuration II. In contrast, the rudder characteristics change due to an additional trim stiffness attached to the rudder pedal mechanism. The equivalent stiffness can simply be calculated by adding the estimated trim stiffness

$c_t = 33.12$ N-m/rad

to the equivalent stiffness of configuration II:

$$c^{III}_{NL,R}(\beta) = c^{II}_{NL,R}(\beta) + c_t \qquad \text{(B5)}$$

For no damping in the trim stiffness, the damping loss angle changes to

$$\gamma^{III}_{NL,R}(\beta) = \frac{\gamma^{II}_{NL,R}(\beta)\ c^{II}_{NL,R}(\beta)}{c^{II}_{NL,R}(\beta) + c_t} \tag{B6}$$

Both $c^{III}_{NL,R}(\beta)$ and $\gamma^{III}_{NL,R}(\beta)$ are shown in figure 15.

Artificial Linear Configuration

Finally, the properties of the artificial linear elements were determined by means of dynamic tests to be

$$\gamma_{L,A} \sim 0.310 \qquad \gamma_{L,R} \sim 0.272$$

$$c_{L,A} = 51.25 \text{ N-m/rad} \qquad c_{L,R} = 21.4 \text{ N-m/rad}$$

Thus, all the data are known to set up the nonlinear equations of motion (eq. (15)).

REFERENCES

1. Breitbach, E.: Effects of Structural Non-Linearities on Aircraft Vibration and Flutter. AGARD-R-665, Jan. 1978.

2. Freymann, Raymond: Bestimmung der dynamischen Aktuatorübertragungsfunktionen mit Hilfe eines experimentell-rechnerischen Verfahrens. Z. Flugwiss. Weltraumforsch., Bd. 2, Heft 6, 1978, pp. 405-416.

3. Haidl, G.: Non-Linear Effects in Aircraft Ground and Flight Vibration Tests. AGARD-R-652, Dec. 1976.

4. Sensburg, Otto; and Schoen, Beate: Schwingung- und Flatteranalyse von Flugzeugen mit besonderen nichtlinearen Struktureigenschaften. Z. Flugwiss. Weltraumforsch., Bd. 2, Heft 6, 1978, pp. 395-404.

5. Breitbach, E.: Flattersimulation des Flugzeuges mit Hilfe des elektronischen Analogrechners unter besonderer Berücksichtigung struktureller Nichtlinearitäten. DLR-FB 73-30, 1973. (Available in English as ESRO TT-121, Dec. 1974.)

6. Breitbach, Elmar J.: Treatment of the Control Mechanisms of Light Airplanes in the Flutter Clearance Process. Science and Technology of Low Speed and Motorless Flight, NASA CP-2085, Pt. II, 1979, pp. 437-466.

7. Woolston, Donald S.; Runyan, Harry L.; and Andrews, Robert E.: An Investigation of Effects of Certain Types of Structural Nonlinearities on Wing and Control Surface Flutter. J. Aero. Sci., vol. 24, no. 1, Jan. 1957, pp. 57-63.

8. Bogoliubov, N. N.; and Mitropolsky, Y. A.: Asymptotic Methods in the Theory of Non-Linear Oscillations. Gordon & Breach Sci. Publ., Inc., 1961.

9. Laurenson, Robert M.; and Trn, Robert M.: Flutter Analysis of Missile Control Surfaces Containing Structural Nonlinearities. A Collection of Technical Papers on Design and Loads - AIAA/ASME/ASCE/AHS 20th Structures, Structural Dynamics, and Materials Conference, Apr. 1979, pp. 352-359. (Available as AIAA Paper 79-0796.)

10. Gelb, Arthur; and Vander Velde, Wallace E.: Multiple-Input Describing Functions and Nonlinear System Design. McGraw-Hill Book Co., c.1968.

11. Iwan, W. D.; and Patula, E. J.: The Merit of Different Error Minimization Criteria in Approximate Analysis. Trans. ASME, Ser. E: J. Appl. Mech., vol. 39, no. 1, Mar. 1972, pp. 257-262.

12. Spanos, P-T. D.; and Iwan, W. D.: Harmonic Analysis of Dynamic Systems With Nonsymmetric Nonlinearities. Trans. ASME, Ser. G: J. Dyn. Syst., Meas., & Control, vol. 101, no. 1, Mar. 1979, pp. 31-36.

TABLE I.- STRIP SCHEME AND FIVE ANTISYMMETRICAL NORMAL MODE SHAPES FOR WING

Strip no.		1	2	3	4	5	6	7	8	9	10
Width, s, cm		30	157.5	150	103.5	50	50	50	50	50	59
Half-chord length of wing, ℓ, cm . . .		46.38	44.56	41.76	39.44	36.50	33.50	30.50	27.50	24.50	21.23
Aileron chord length ratio, τ_A		0	0	0	0	0.264	0.272	0.280	0.288	0.296	0
Mode r = 1	h, cm	0	0	0	0	0	0	0	0	0	0
	α, rad	0	0	0	0	0	0	0	0	0	0
	β, rad	0	0	0	0	0	0	0	0	0	0
Mode r = 2	h, cm	-0.0094	-0.0269	-0.0263	-0.0356	-0.0363	-0.0325	-0.0250	-0.0125	-0.0060	0.0060
	α, rad	0	0	0	0	0	0	0	0	0	0
	β, rad	0	0	0	0	0.0513	0.0520	0.0528	0.0535	0.0560	0
Mode r = 3	h, cm	0.0063	0.0356	0.0450	0.0063	-0.0375	-0.0825	-0.1340	-0.1950	-0.2640	-0.3470
	α, rad	0	0	0	0	0	0	0	0	0	0
	β, rad	0	0	0	0	0.0520	0.0540	0.0555	0.0560	0.0560	0
Mode r = 4	h, cm	0.0281	0.1710	0.3330	0.2720	0.1250	-0.0188	-0.1980	-0.4420	-0.7360	-1.110
	α, rad	0	0	0	0	0	0	0	0	0	0
	β, rad	0	0	0	0	0	0	0	0	0	0
Mode r = 5	h, cm	0	0	0	0	0	0	0	0	0	0
	α, rad	0	0	0	0	0	0	0	0	0	0
	β, rad	0	0	0	0	0	0	0	0	0	0

TABLE II.- STRIP SCHEME AND FIVE ANTISYMMETRIC NORMAL MODE SHAPES FOR ELEVATOR

Strip no.		1	2	3	4	5
Width, s, cm		7.5	32.5	30	30	30
Half-chord length of elevator, ℓ, cm		25.75	24.5	23.25	20.81	19.69
Mode r = 1	h, cm	0	0	0	0	0
	α, rad	0	0	0	0	0
Mode r = 2	h, cm	-0.0125	-0.0188	-0.0513	-0.0806	-0.0844
	α, rad	0.0008	0.0008	0.0013	0.0017	0.0017
Mode r = 3	h, cm	0.0575	0.1725	0.3581	0.5406	0.7125
	α, rad	-0.0005	-0.0009	-0.0005	-0.0002	-0.0009
Mode r = 4	h, cm	-0.0125	-0.0238	-0.0531	0.0738	-0.0863
	α, rad	0	0	0	0	0
Mode r = 5	h, cm	0.0838	0.2495	0.4969	0.7431	1.0000
	α, rad	0	-0.0005	-0.0012	-0.0013	0

TABLE III.- STRIP SCHEME AND FIVE ANTISYMMETRIC NORMAL MODE SHAPES FOR VERTICAL TAIL

Strip no.		1	2	3	4	5
Width, s, cm		50.64	44.73	37.00	28.60	22.10
Half-chord length of vertical tail, ℓ, cm		20	30	40	31.5	21
Rudder chord length ratio, τ_R		0.443	0.450	0.459	0.469	0
Mode r = 1	h, cm	0.0313	-0.0940	-0.1565	-0.0940	-1.1200
	α, rad	0.0043	-0.0043	-0.0113	-0.0140	0.1020
	β, rad	0.1000	0.1000	0.1000	0.1000	0
Mode r = 2	h, cm	-0.0625	-0.0838	-0.1163	-0.1525	-0.1838
	α, rad	0	0	0	0	0
	β, rad	0	0	0	0	0
Mode r = 3	h, cm	0.2688	0.3975	0.6063	0.8563	1.044
	α, rad	0.0025	0.0025	0.0032	0.0061	0.0085
	β, rad	0	0	0	0	0
Mode r = 4	h, cm	-0.2038	-0.2288	-0.2750	0.3400	-0.3688
	α, rad	-0.0018	-0.0018	-0.0025	-0.0039	-0.0025
	β, rad	0.0024	0.0024	0.0024	0.0040	0
Mode r = 5	h, cm	-0.2063	-0.1325	-0.0250	0.0938	0.1212
	α, rad	-0.0017	-0.0019	-0.0019	-0.0012	0.0058
	β, rad	0.0064	0.0064	0.0064	0.0064	0

TABLE IV.- MODAL CHARACTERISTICS OF THE FIVE LOWEST ANTISYMMETRICAL NORMAL MODES OF A SAILPLANE

Mode, r	M_r, kg-cm^2	f_r, Hz	γ_r	Remarks
1	19.22	1.68	0.272	Rudder
2	3.50	4.90	.310	Aileron
3	12.90	5.39	.042	Tail - aileron
4	15.40	6.69	.019	First antisymmetrical wing bending
5	3.24	8.57	.078	Elevator

TABLE V.- ROW MATRICES CONTAINING HINGE ROTATIONS $\beta_{R,r}$ AND $\beta_{A,r}$ OF RUDDER AND AILERON ACCORDING TO EQUATION (7)

$$\Phi_R = [0.1,0,0,0.0024,0.0064]$$

$$\Phi_A = [0,0.0573,0.0520,0,0]$$

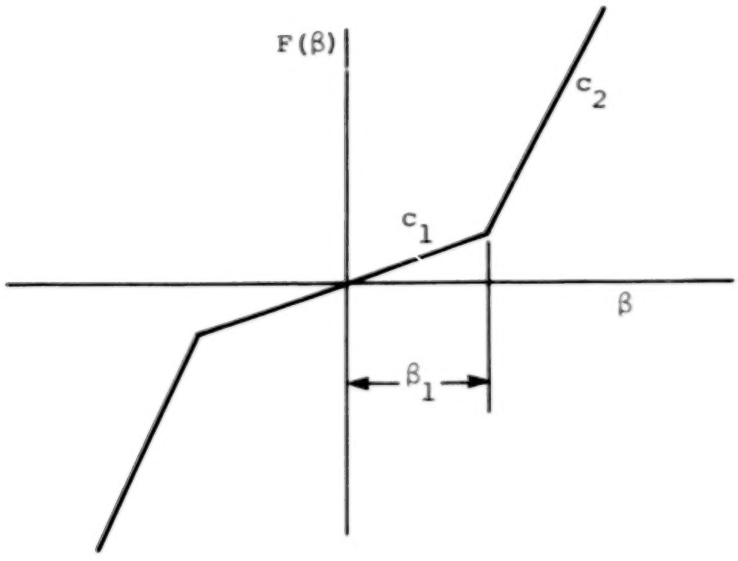

Figure 1.- Bilinear force-deflection diagram without damping.

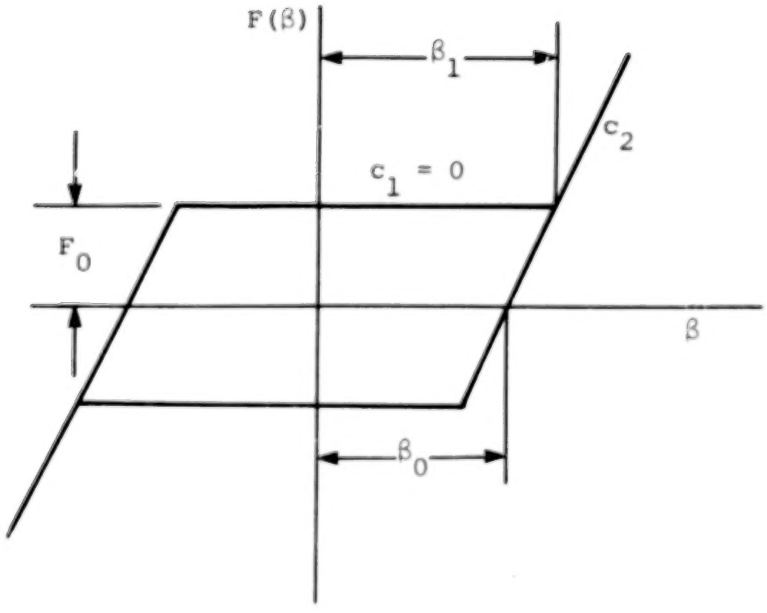

Figure 2.- Bilinear hysteresis-type force-deflection diagram.

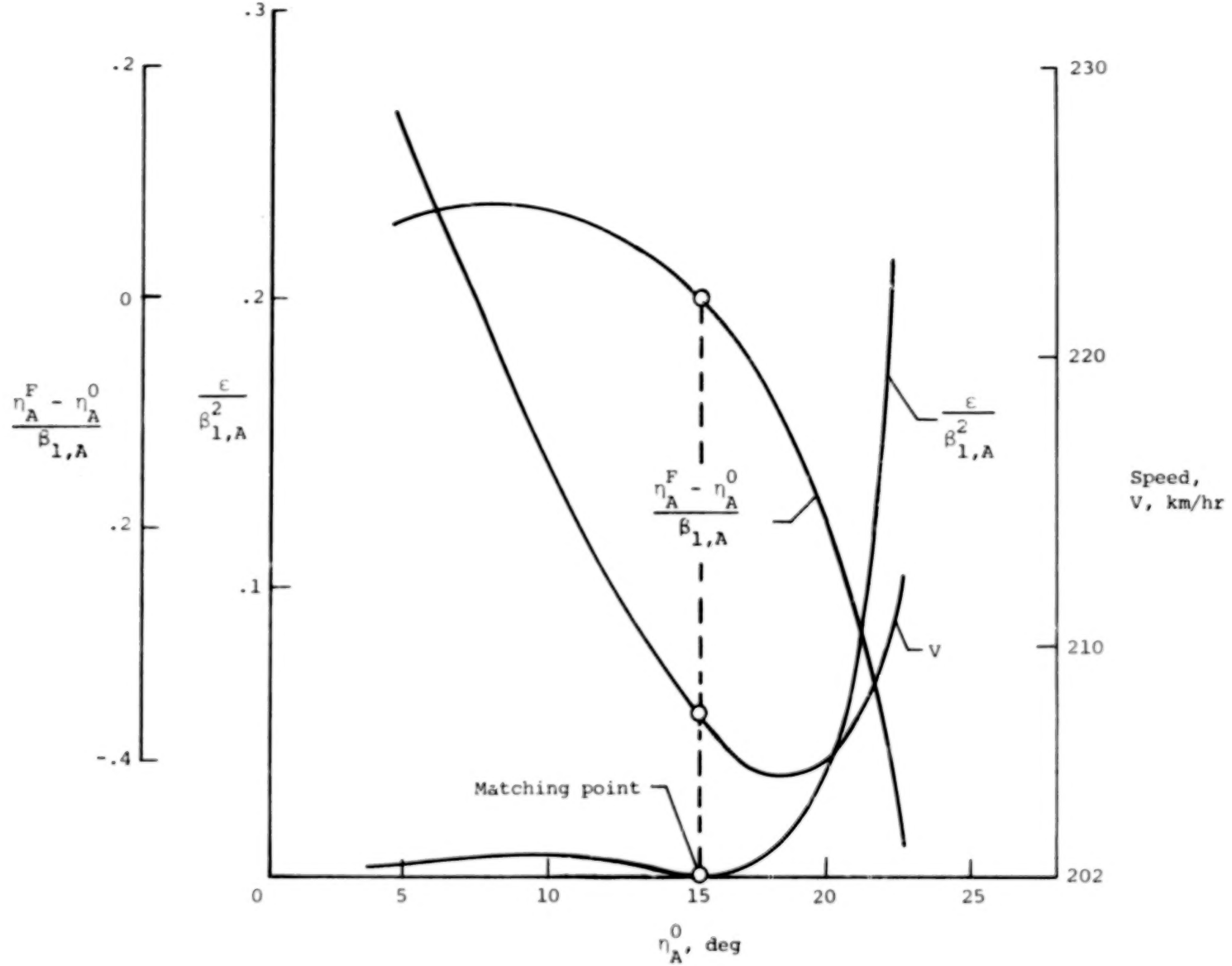

Figure 3.- Some characteristic functions near matching point. Configuration II; $\eta_R^0/\beta_{1,R} = 0.858$.

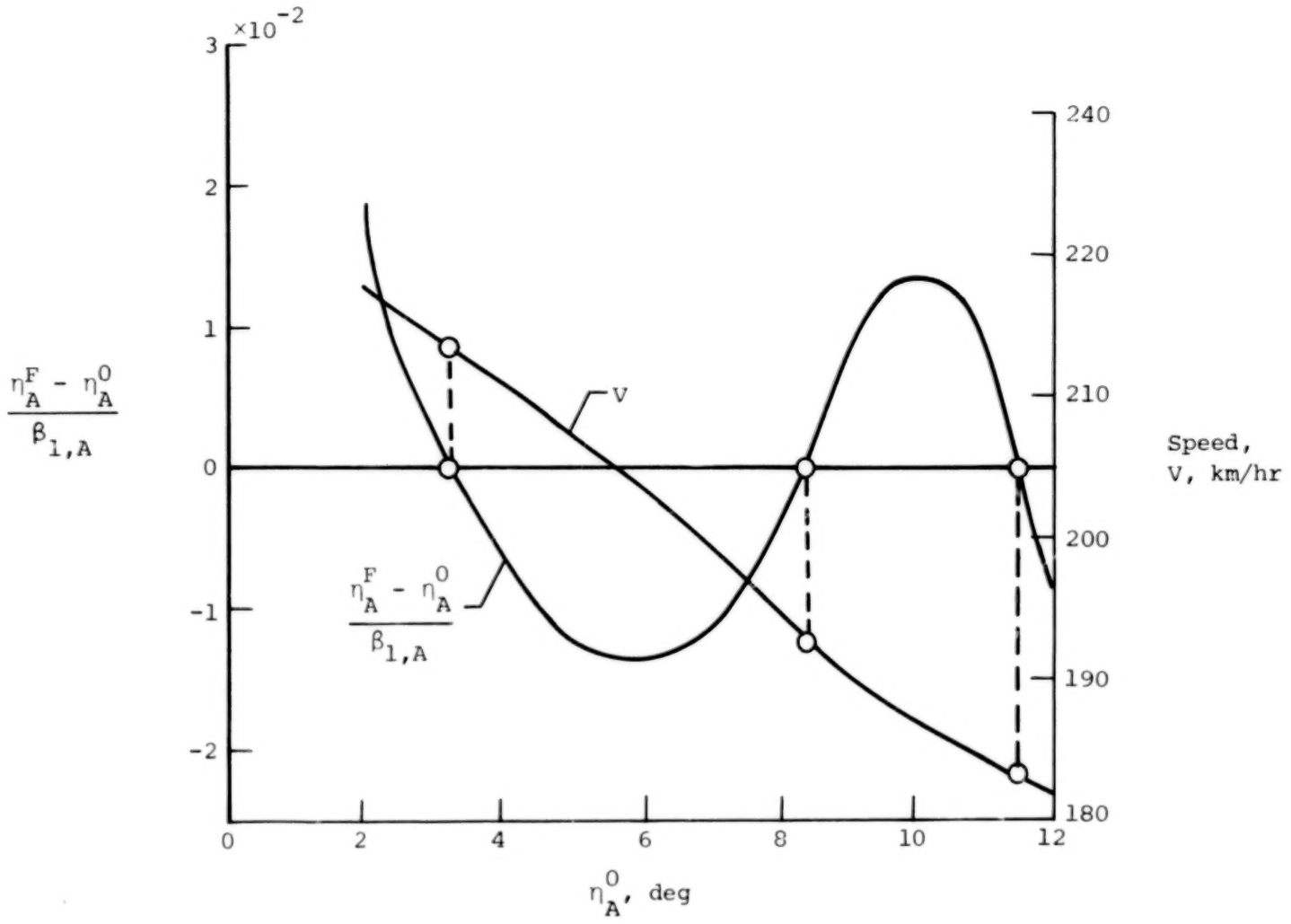

Figure 4.- Functions $(\eta_A{}^F - \eta_A{}^0)/\beta_{1,A}$ and V versus $\eta_A{}^0$ for special case of three different matching points. Configuration III; $\eta_R{}^0/\beta_{1,R} = 0.5$.

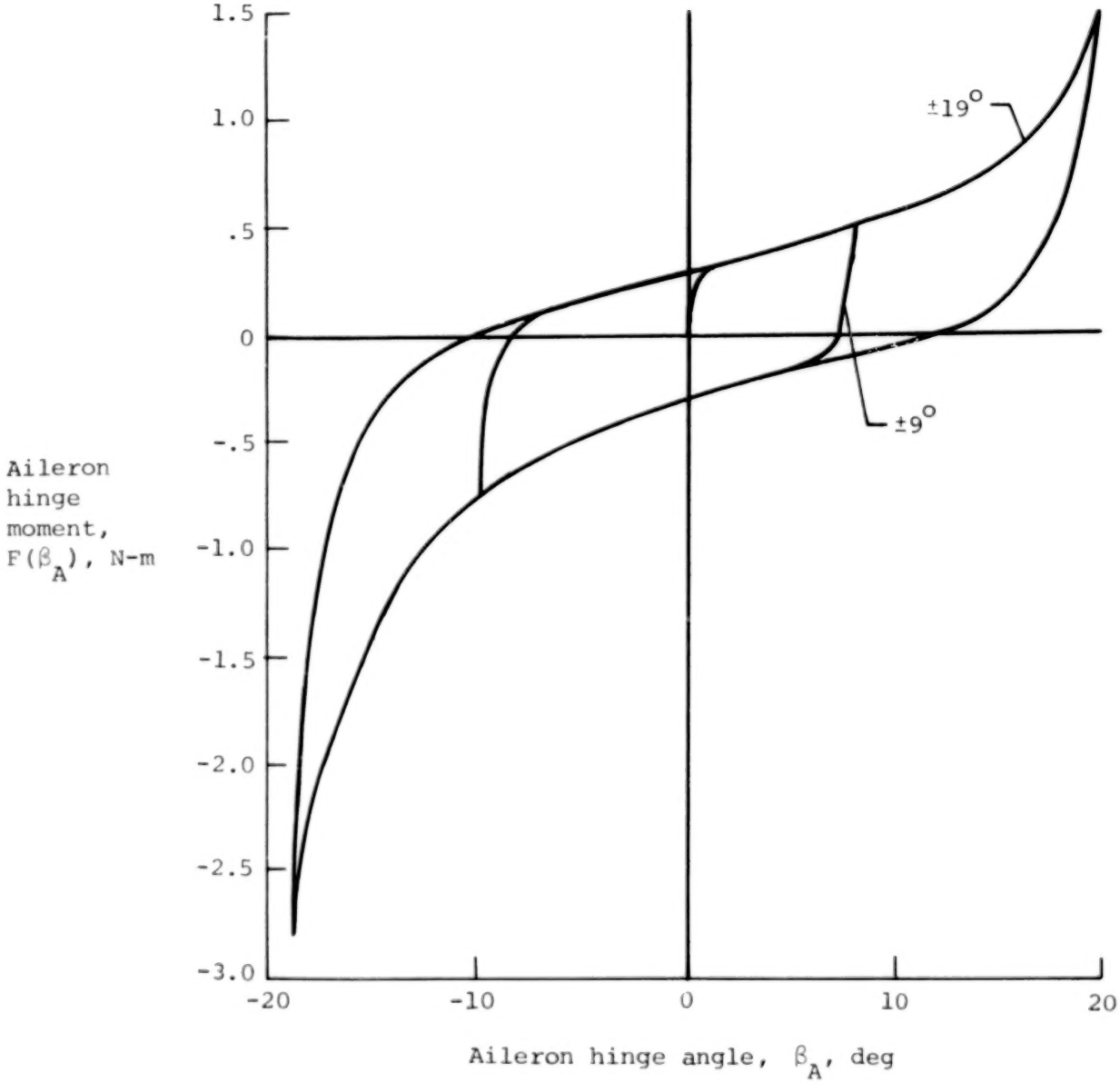

Figure 5.- Measured force-deflection diagram of aileron system for two different amplitudes. Antisymmetrical case.

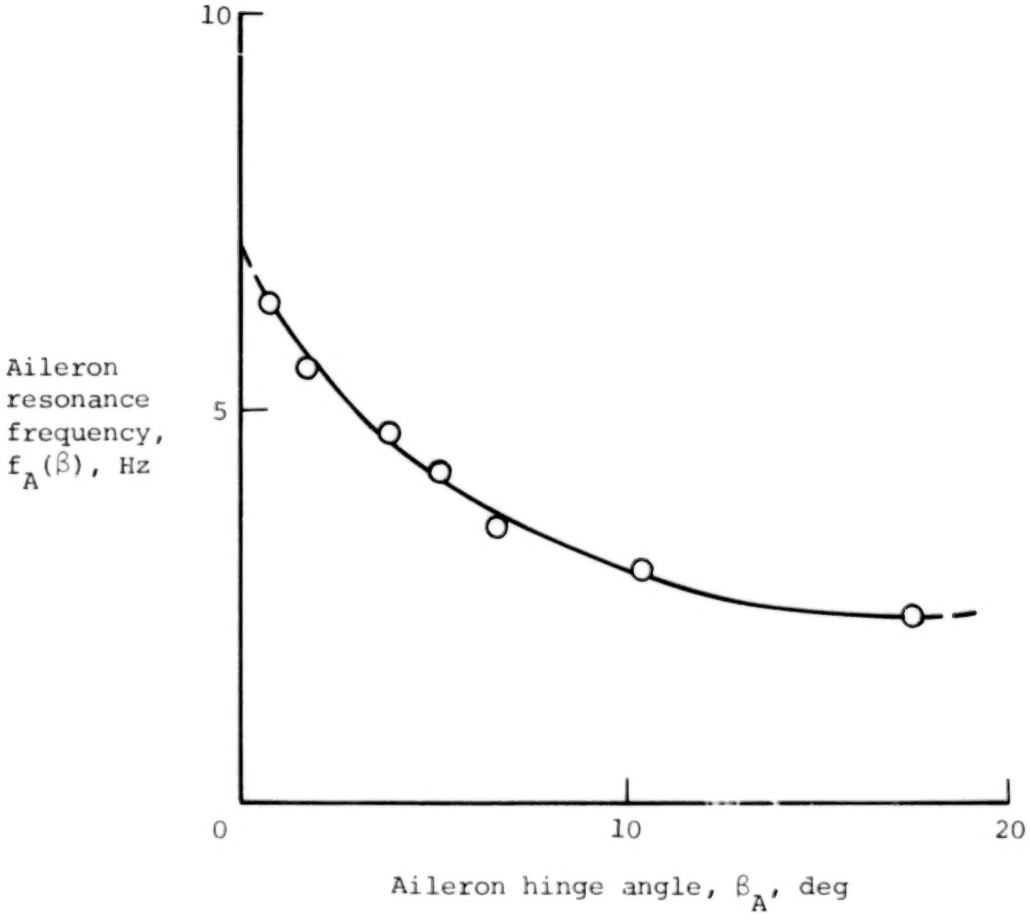

Figure 6.- Measured resonance frequency of antisymmetrical aileron vibration versus hinge angle.

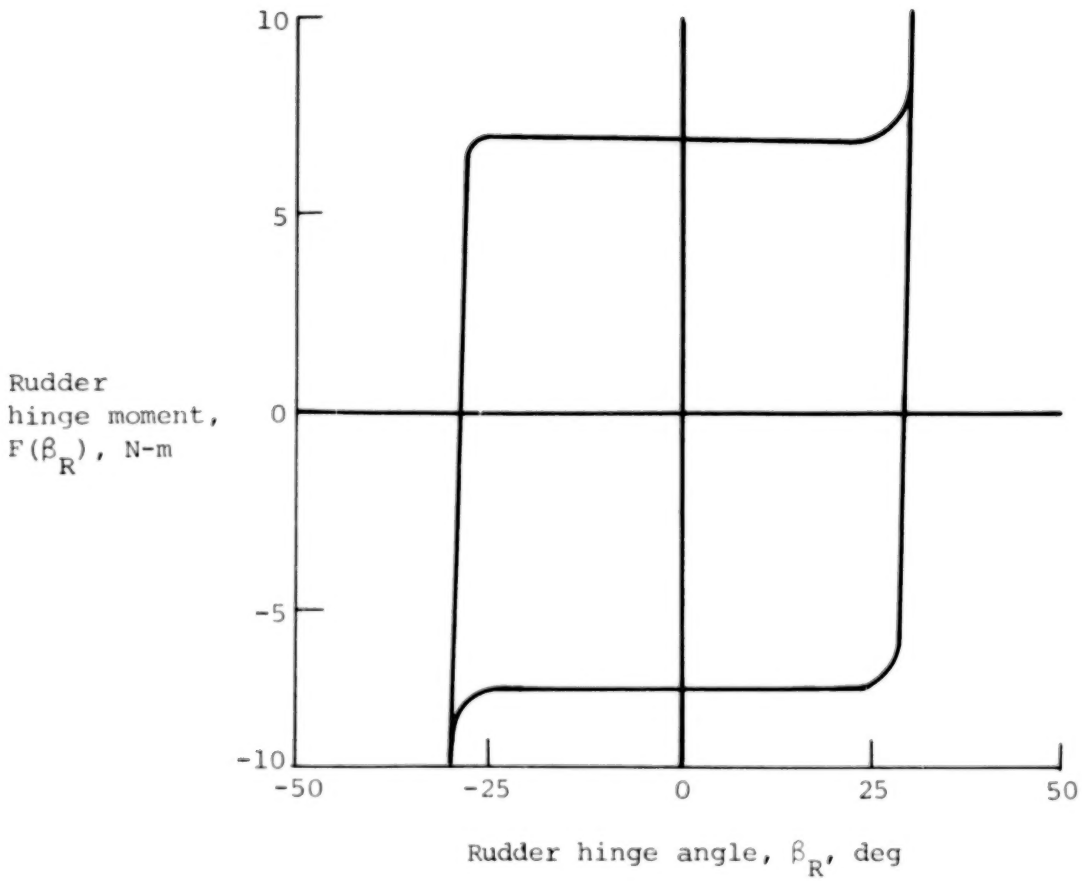

Figure 7.- Measured force-deflection diagram of rudder system with trim stiffness removed.

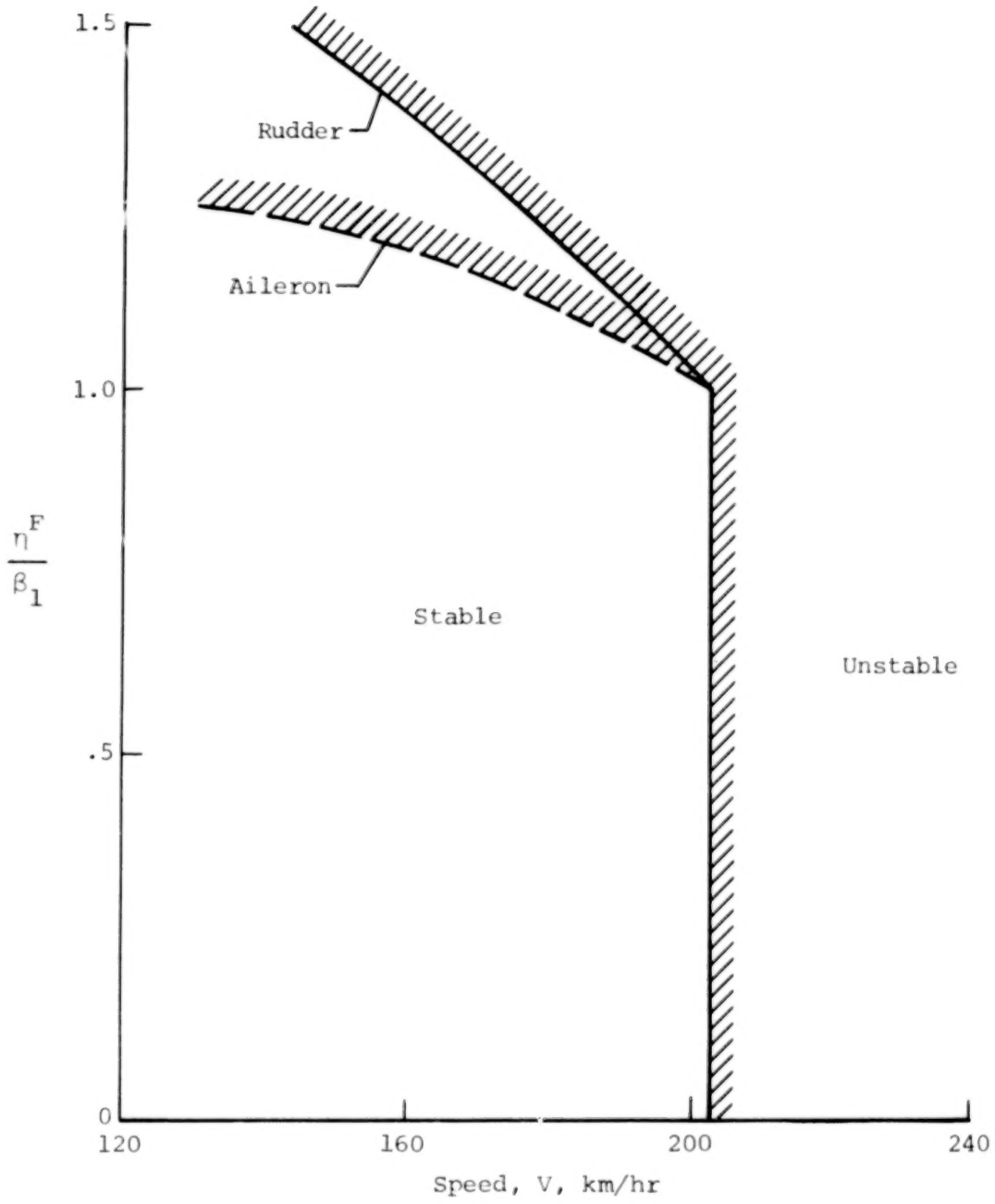

Figure 8.- Nonlinear flutter boundary for configuration I.

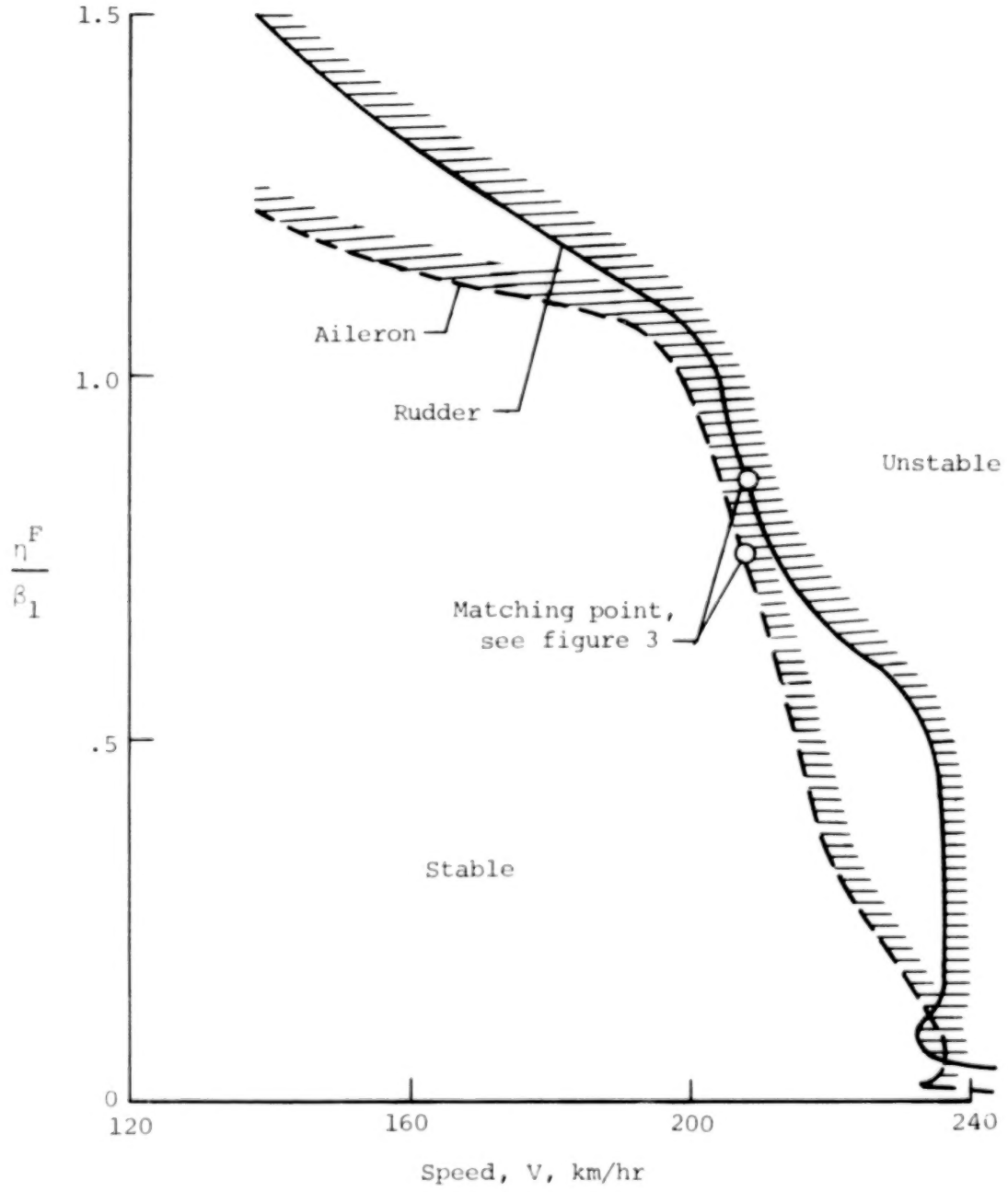

Figure 9.- Nonlinear flutter boundary for configuration II.

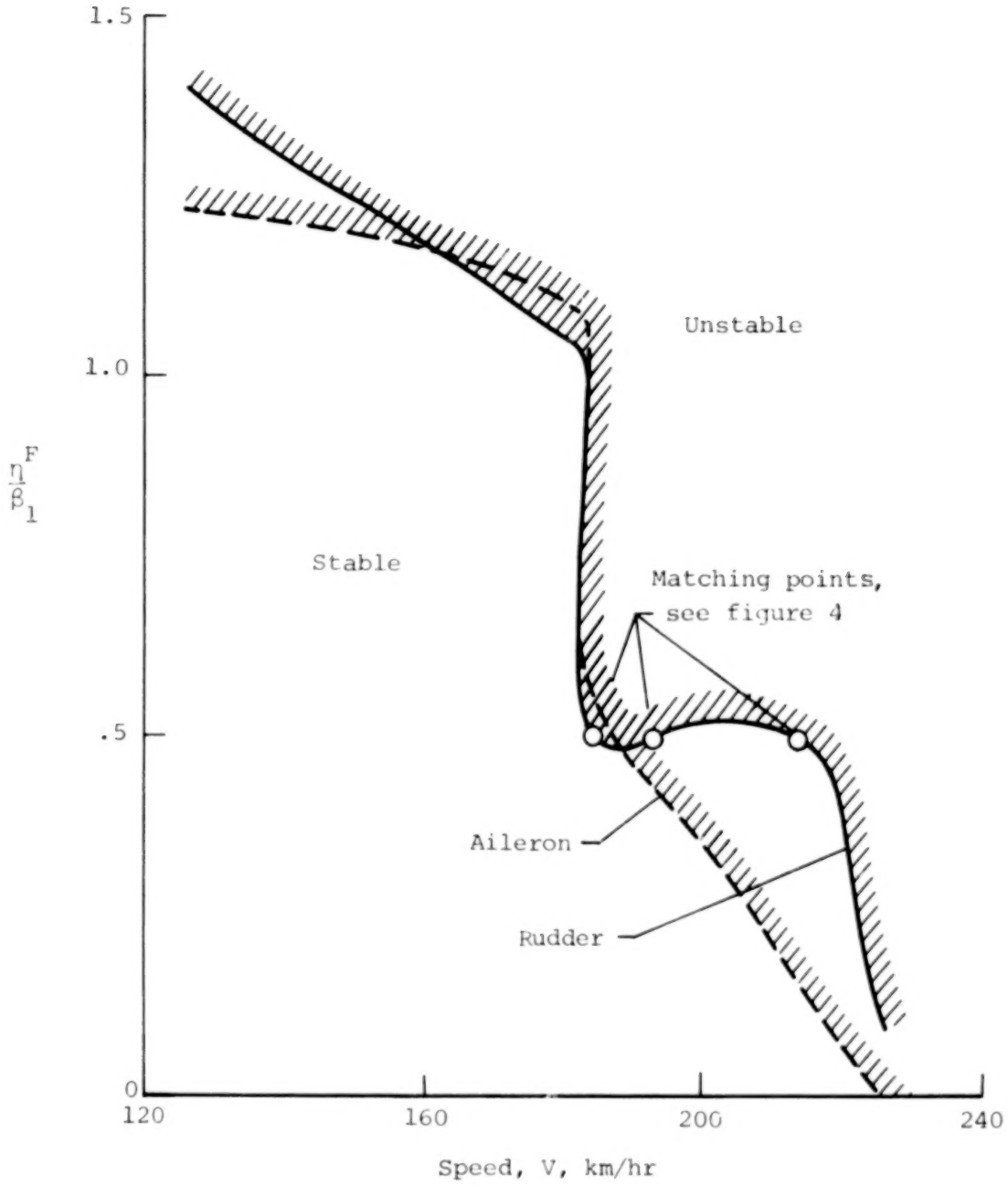

Figure 10.- Nonlinear flutter boundary for configuration III.

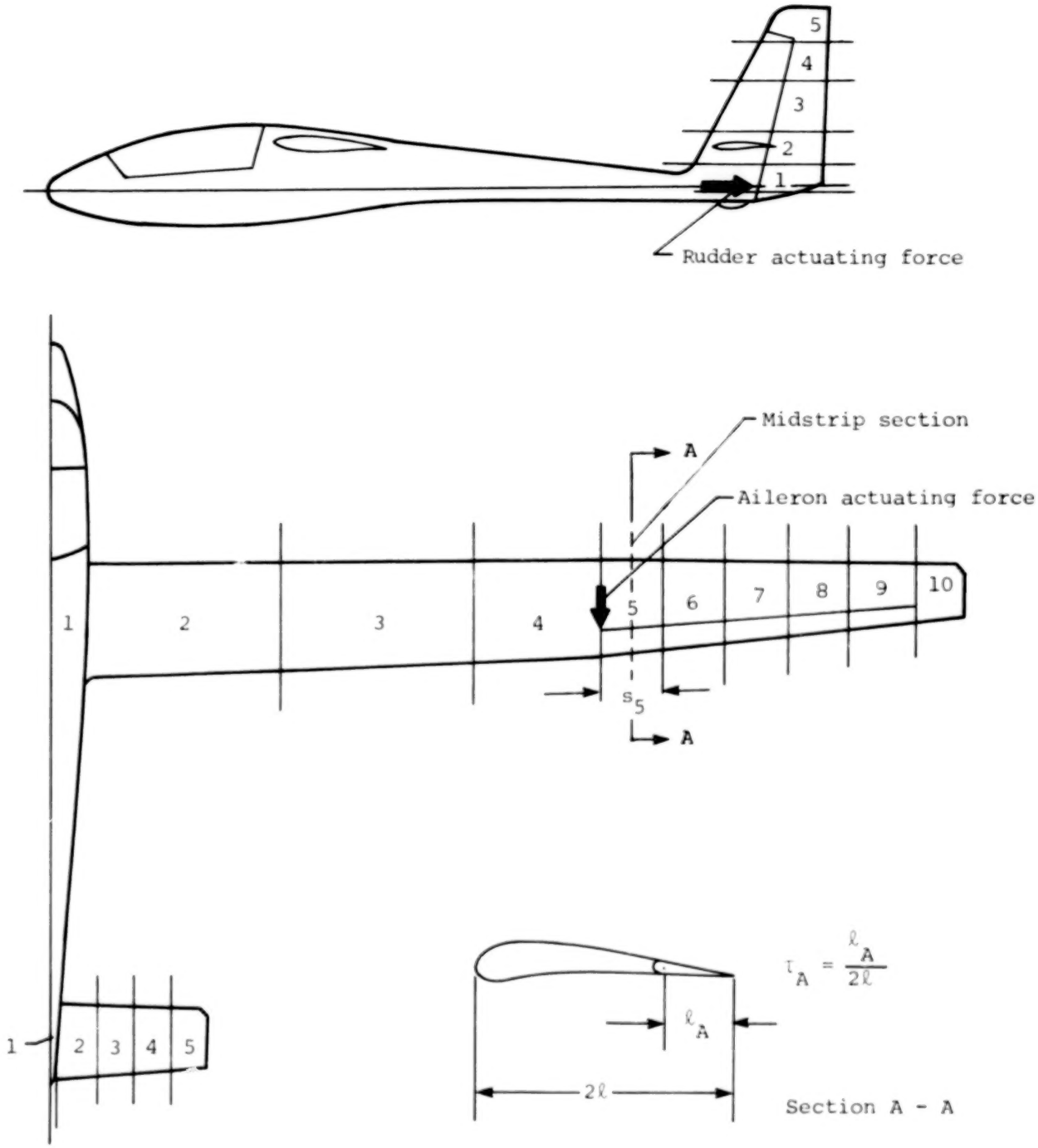

Figure 11.- Schematic view of a sailplane.

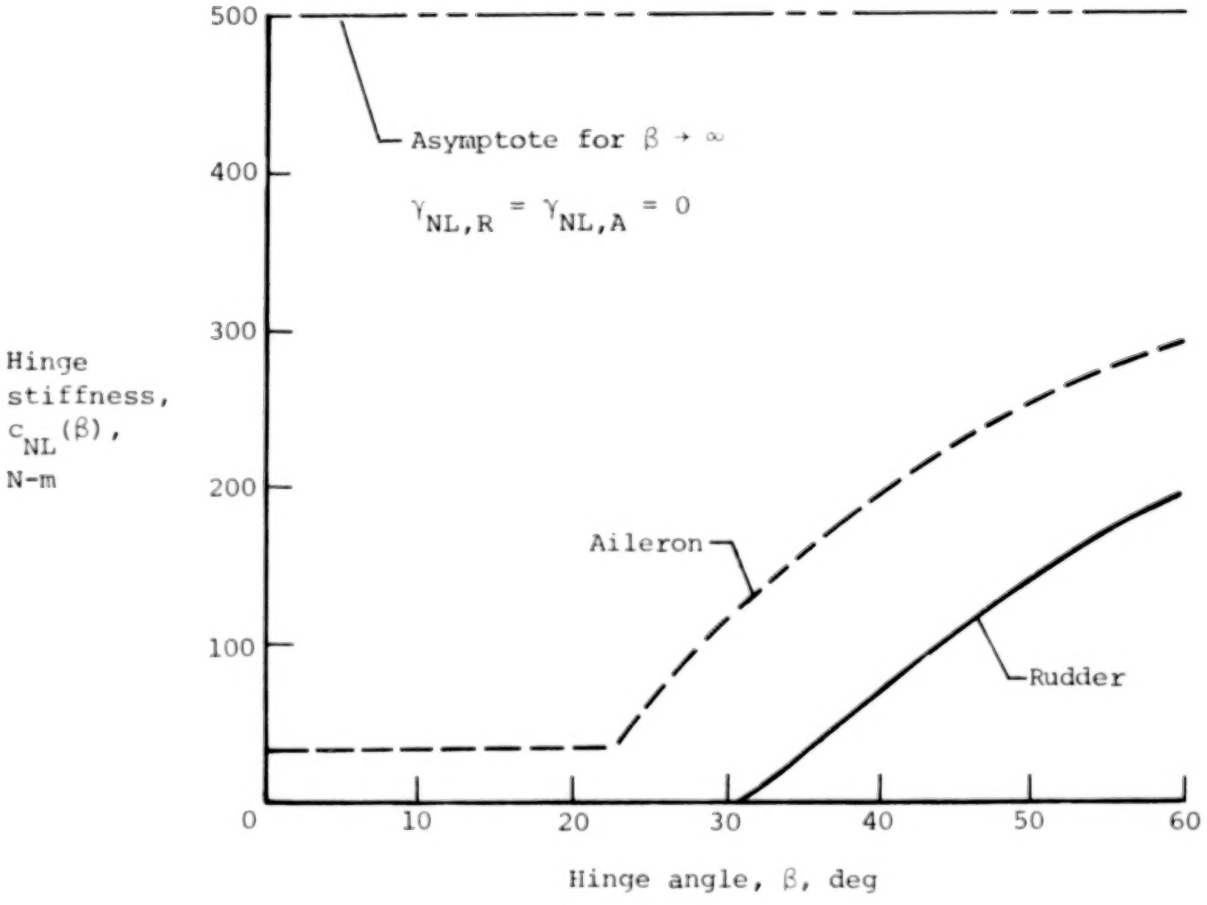

Figure 12.- Hinge stiffness of rudder and aileron versus hinge angle. Configuration I.

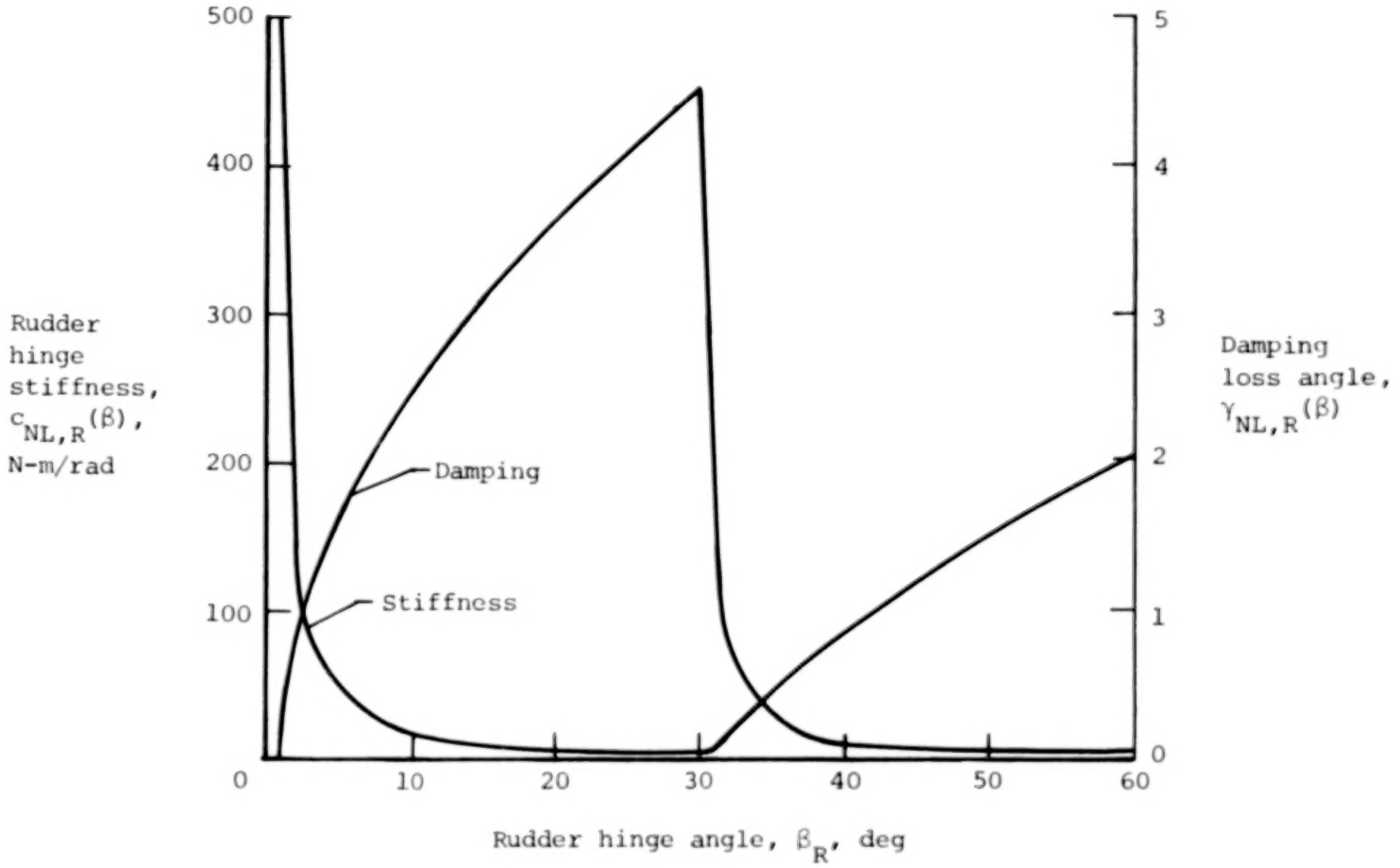

Figure 13.- Hinge stiffness and damping of rudder without trim stiffness versus hinge angle. Configuration II.

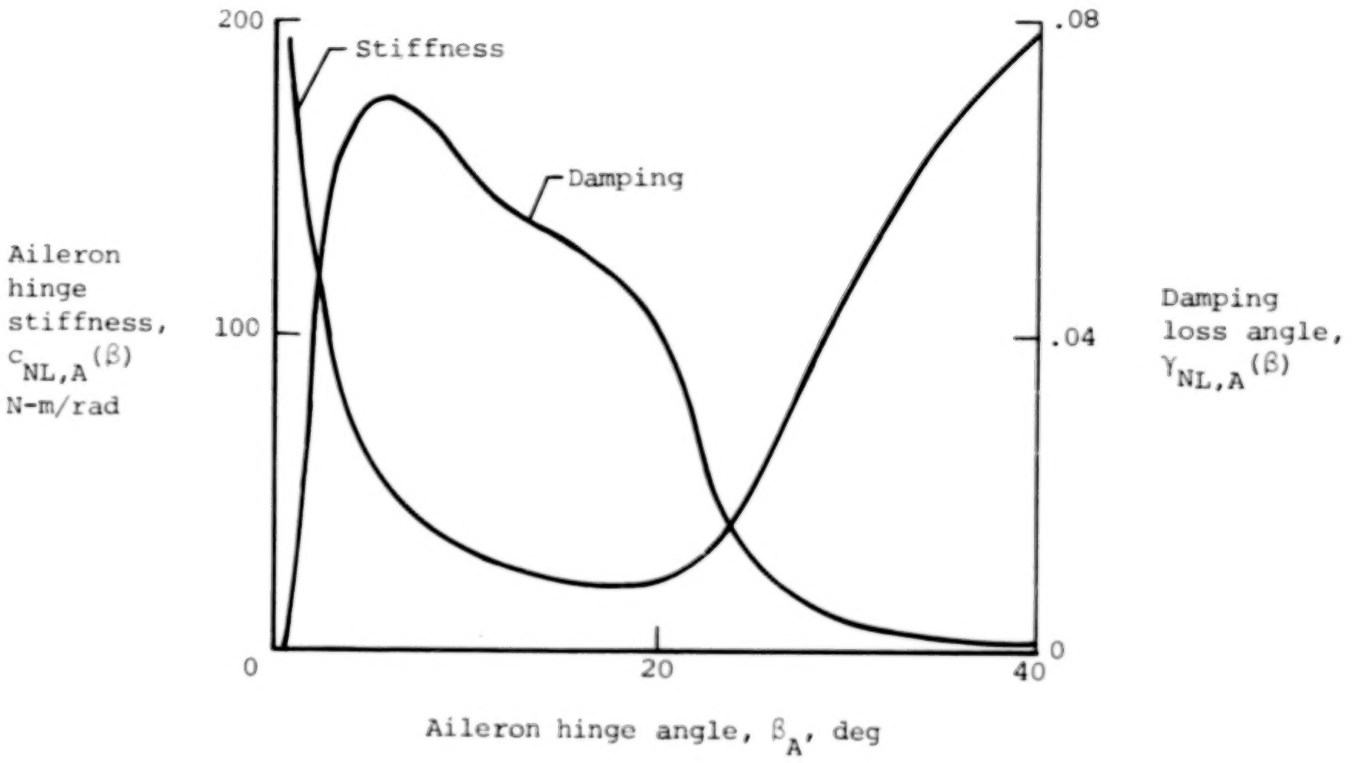

Figure 14.- Aileron hinge stiffness and damping versus hinge angle. Configurations II and III.

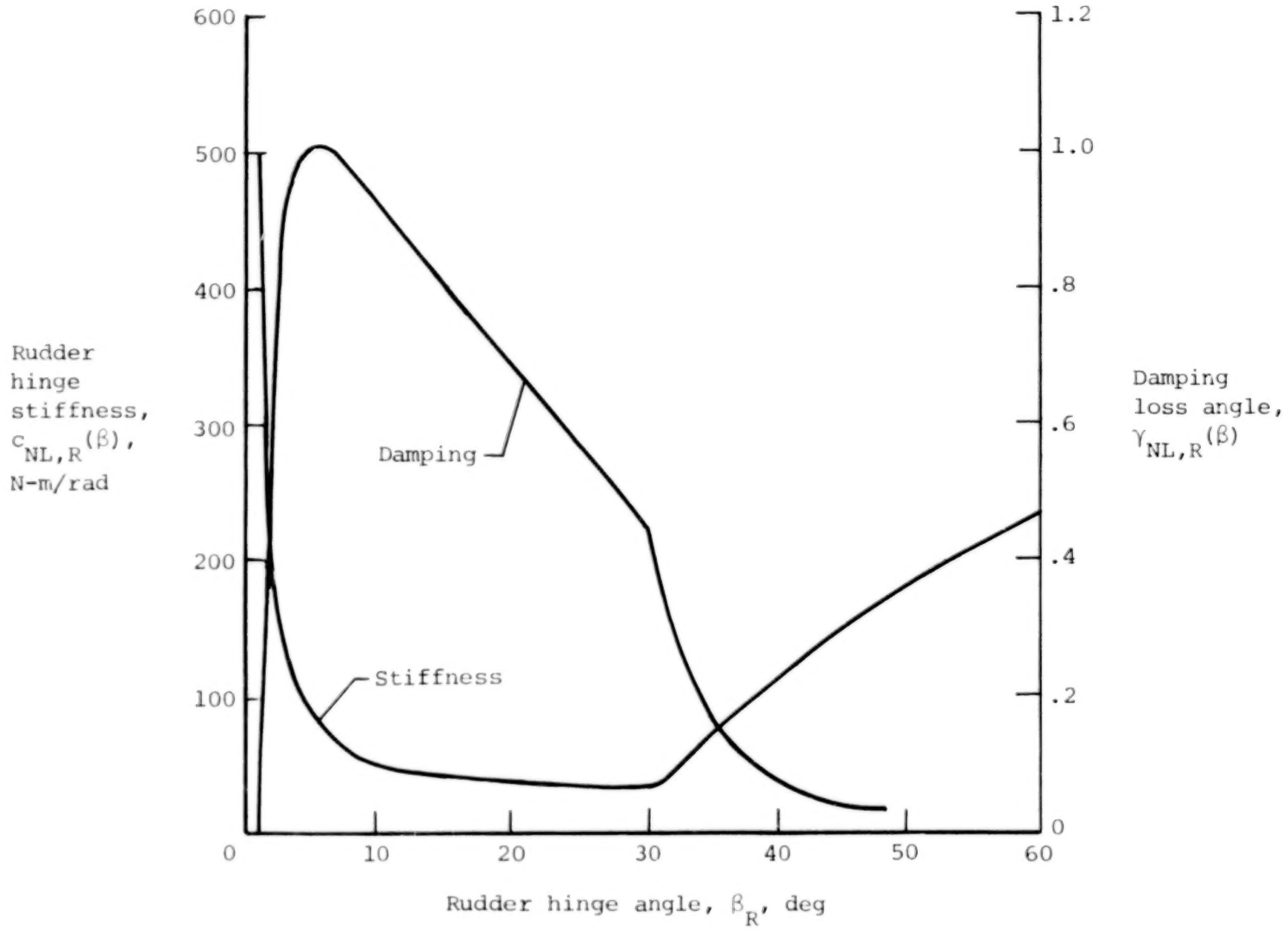

Figure 15.- Hinge stiffness and damping of rudder with trim stiffness versus hinge angle. Configuration III.

1. Report No.	2. Government Accession No.	3. Recipient's Catalog No.
NASA TP-1620		

4. Title and Subtitle	5. Report Date
FLUTTER ANALYSIS OF AN AIRPLANE WITH MULTIPLE STRUCTURAL NONLINEARITIES IN THE CONTROL SYSTEM	May 1980
	6. Performing Organization Code

7. Author(s)	8. Performing Organization Report No.
Elmar J. Breitbach	L-13356
	10. Work Unit No. 505-33-53-01

9. Performing Organization Name and Address	11. Contract or Grant No.
NASA Langley Research Center Hampton, VA 23665	
	13. Type of Report and Period Covered Technical Paper

12. Sponsoring Agency Name and Address	14. Sponsoring Agency Code
National Aeronautics and Space Administration Washington, DC 20546	

15. Supplementary Notes

Elmar J. Breitbach: NRC-NASA Senior Resident Research Associate, now at DFVLR, Institut für Aeroelastik, Göttingen, West Germany.

16. Abstract

Experience has shown that the flutter prediction process for airplanes can be greatly affected by strong concentrated nonlinearities which may be localized in the linking elements of the control mechanism, in the pivot joints of variable-sweep-wing systems, and in the connecting points between wing- and pylon-mounted external stores. The principle of equivalent linearization offers an efficient possibility for solving the related nonlinear flutter equations in the frequency domain as a complement to the well-known time domain procedures. Taking as an example an airplane with nonlinear control characteristics, it is demonstrated how the equivalent linearization approach can be extended to rather complicated systems with multiple sets of strongly interacting, concentrated nonlinearities.

17. Key Words (Suggested by Author(s))	18. Distribution Statement
Flutter Nonlinear Control	Unclassified - Unlimited Subject Category 08

19. Security Classif. (of this report)	20. Security Classif. (of this page)	21. No. of Pages	22. Price*
Unclassified	Unclassified	36	$4.50

For sale by the National Technical Information Service, Springfield, Virginia 22161

NASA-Langley, 1980

90 %

50 %